Article

Impact of Grounding Modeling on Lightning-induced Voltages Evaluation in Distribution Lines

Daniele Mestriner[1,†], Rodolfo Antônio Ribeiro de Moura [2,†,*], Renato Procopio [3,†] and Marco Aurélio de Oliveira Schroeder [4,†]

[1] Naval, ICT and Electrical Engineering Department (DITEN), University of Genoa, Via Opera Pia 11a, Genoa, Italy; daniele.mestriner@edu.unige.it
[2] Electrical Engineering Department - Federal University of São João del-Rei; moura@ufsj.edu.br
[3] Naval, ICT and Electrical Engineering Department (DITEN), University of Genoa, Via Opera Pia 11a, Genoa, Italy; renato.procopio@unige.it
[4] Electrical Engineering Department - Federal University of São João del-Rei; schroeder@ufsj.edu.br
* Correspondence: moura@ufsj.edu.br; Tel.: +55 32 99102 0091
† These authors contributed equally to this work.

Abstract: Lightning-induced voltages are one of the main causes of shutdown in distribution lines. In this work, attention is focused on the effects of wideband modeling of electric grounding in the overvoltage calculation along insulator strings due to indirect lightning strikes. This study is done directly in the time-domain with the grounding being represented with an equivalent circuit accounting for its dynamics. Results show that the adoption of commonly adopted simplified grounding models, such as low-frequency resistance, may lead to an underestimation of the overvoltage. According to results, differences in the order of 30% can be found in some studied cases.

Keywords: Distribution Lines; lightning-induced overvoltages; grounding modeling; soil resistivity

Citation: Mestriner, D.; Procopio, R.; Moura, R. A. R.; Schroeder, M. A. O.; Evaluation of the impact of grounding modeling on lightning-induced in distribution lines. *Journal Not Specified* **2021**, *1*, 0. https://dx.doi.org/

Received:
Accepted:
Published:

1. Introduction

Transmission and Distribution Lines are highly affected and damaged by direct and indirect lightning events. Direct events occur when the lightning directly strikes the line; such events are hazardous but rare and are typically studied and analyzed in the framework of Transmission Lines (TL). On the other side, indirect events occur when lightning strikes the ground in the proximity of a power system; these events are much more frequent with respect to direct ones, but the overall voltage induced in the power system is usually much lower. For this reason, indirect events are not of interest for TL since the induced voltages are generally lower than the line Critical-Flash-Over (CFO) voltage, but they are vital when dealing with Distribution Lines (DL), which are characterized by a low CFO.

Most works address lightning-induced voltages in DL model electric grounding as a constant value resistance R_{LF} [1–16]. This parameter is associated with a low-frequency behavior, i.e., disregarding its electromagnetic dynamic. Therefore, this low-frequency grounding resistance cannot reproduce the reactive (inductive and capacitive) and electromagnetic wave propagation effects (attenuation and distortion), prominent in the high-frequency range related to the voltage and current wavefronts. Additionally, the determination of overvoltage on TL, due to direct lightning, is highly sensible on the electromagnetic modeling of the electrical grounding [17].

In view of the above, this work presents an evaluation of the impact of grounding modeling on lightning-induced voltage. Thus, the main original contribution of this paper is to include, in the time domain type simulations, an equivalent electric circuit that reproduces the complete frequency response of grounding, with full inclusion of the aforementioned effects. The Hybrid Electromagnetic Model (HEM) is used to determine the wideband grounding frequency response $Z(\omega)$ [18,19]. To implement the $Z(\omega)$ *in silico*, the Vector Fitting (VF) technique is applied to generate an equivalent electric circuit that is easily inserted in EMT-type software [20,21]. In the following, the grounding circuit will be implemented in the software developed in [22].

The results illustrate that the induced voltages, considering the grounding modeled via R_{LF} are quite different from those results using $Z(\omega)$, with perceptual differences reaching values of around 30%. It is noticeable that the differences increase with the soil resistivity and with the point of occurrence of the lightning (lightning striking closer to the DL increase the perceptual differences) for both first and subsequent return strokes. The paper is organized as follows: Sections 2, 3 and 4 show the lightning field-to-line coupling problem equations, the tower and the grounding modeling, respectively; while Sections 5 and 6 present the test cases and the results. Section 7 is dedicated to the conclusions.

2. Induced-lightning modeling

The lightning-induced voltages occurring in a DL are here evaluated, recalling the procedure presented in [22] and [23]. This procedure is usually divided into two steps: i) the ElectroMagnetic (EM) fields computation and ii) the field-to-line coupling.

2.1. EM fields computation

The EM fields are computed analytically thanks to the approach proposed in [24] and validated in [25]. The method requires as input the knowledge of the channel-base current, the return stroke height and the return stroke velocity. It can be applied both to perfect electric conductor ground and soil characterized by a finite conductivity. The only assumption required is the TL model for the attenuation of the current along the channel. The main advantage of this approach consists of the possibility of dealing with analytical formulas, which guarantee a fast solution and a low computational effort.

2.2. Field-to-line coupling

The field-to-line coupling computation is obtained thanks to the well-known Agrawal model [26], which is here presented in its extended version taking into account the presence of a finite-conducting ground and a multi-conductor line.

$$\begin{cases} \frac{\partial V_i^s}{\partial x}(x,t) + \sum_{j=1}^{M} L_{ij}\frac{\partial I_j}{\partial t}(x,t) + V_i^g(x,t) = E_{inc,x,i}(x,t) \\ \frac{\partial I_i}{\partial x}(x,t) + \sum_{j=1}^{M} C_{ij}\frac{\partial V_j^s}{\partial t}(x,t) = 0 \end{cases} \tag{1}$$

with

$$V_i^g(x,t) = \int_0^t \xi_g^i(t-s)\frac{\partial I_i}{\partial s}(x,s)ds \tag{2}$$

where $V_i^s(x,t)$, $I_i(x,t)$ and $E_{inc,x,i}(x,t)$ are the scattered voltage, the current and the tangential component of the exciting electric field (computed in the previous subsection) on the ith conductor at distance x from the beginning of the line. As expressed in equation (1), the knowledge of the inductance and capacitance matrices (L and C) is required. Please note that ξ_i^g is the time-domain expression for the ground impedance [27].

The total voltage occurring on the i-th conductor at the point x can be then expressed as the sum of the scattered voltage and the incident voltage, whose value depends on the vertical electric field (computed in the previous subsection).

The proposed methodology is adapted to an EMT-type software (in this framework Simulink-Simscape is used), through the finite-difference time-domain (FDTD) technique. In this case, a second-order scheme is adopted with $dt = 10ns$ and $dx = 9m$, which satisfies the well-known Courant stability condition. Further details can be found in [22].

3. Tower modeling

The modeling of the tower is usually neglected in lightning-induced voltages studies. However, in this framework, the tower is included in the model according to [28,29] and is modeled as a lossless transmission line, whose characteristic impedance is:

$$Z_c = 60\left[\ln\left(\sqrt{2}\frac{2h}{r}\right) - 1 + \frac{r}{4h} + \left(\frac{r}{4h}\right)^2\right] \tag{3}$$

h being the tower height and r the tower radius. The insulators are modeled as open circuits.

4. Electrical grounding modeling

In this paper, the grounding transient behavior is modeled by HEM [18,19]. This model is an electromagnetic computational method developed for the numerical solution of lightning problems and, according to Cigrè [30], it is classified as a hybrid electromagnetic-circuit approach. The main motivations for using HEM are as follows: i) it is accurate and flexible, i.e., it can be used in different types of grounding configuration; ii) its results have been extensively validated experimentally, such as measurements in TL [18,19], horizontal electrodes [18,31], vertical rods [31,32], and typical substation grounding grids [33] and iii) it is faster than traditional full-wave methods (without losing accuracy). It is worth mentioning that the usage of HEM has increased significantly recently [30,34,35].

Basically, HEM consists of subdividing the actual system (in this case, electrical grounding) into N small conductive cylindrical segments and, for each segment, the electromagnetic theory is applied. After that, with the help of the circuit theory, it is possible to obtain a matrix system that computes the wideband response of the electrical grounding. For the sake of clarity, we present a brief overview of HEM below. More details about HEM are described in [18,19].

It is worthwhile to comment that HEM corresponds to an electromagnetic model developed in the frequency domain. Thus, it is necessary first to determine the frequency spectrum (depending on the phenomenon of interest). After that, the electrical grounding is divided into N segments, where the length of each segment is equal to 10 times its radius (thin wire approximation). A discussion about segmentation length is presented in [36].

Each segment is considered a source of two currents, one longitudinal that flows along the electrode (I_L) and another transversal that flows from the electrode to the surrounding soil (I_T). It is worth noting that I_L generates a non-conservative electric field and I_T a conservative one. With the aid of the magnetic vector and electric scalar potentials, both voltage drops (ΔV) and electric potentials (V) in each pair of segments (transmitter and receiver) are determined. Additionally, double integral equations are established for ΔV and V. These integrals depend on the frequency, geometry, soil parameters and I_T and I_L distributions. However, the distributions of I_T and I_L are not known and are integrands of the integrals. From this point on, the Method of Moments (MoM) is applied to solve these integral equations [37]. The effect of the air-soil interface is included using the method of images, similar to [38,39].

The I_T and I_L distributions considered in this paper are of the piecewise-constant function type [18,19]. MoM makes it possible to transform integral equations into algebraic ones, the solution of which allows determining all the quantities of interest (in the frequency domain), such as I_T, I_L,ΔV and V distributions; transverse (capacitive and conductive couplings) and longitudinal (resistive and inductive couplings) impedances (self and mutual); electromagnetic field; harmonic grounding impedance ($Z(\omega)$); low-frequency grounding resistance (R_{LF}), etc.

As specified before, the calculation of induced voltages is performed directly in the time domain; however $Z(\omega)$ is a frequency domain quantity. Thus, the well-known Vector Fitting (VF) approach is used for fitting the calculated frequency domain grounding response with rational function approximations [20]. The passivity is enforced by perturbation [21].

Finally, based on the obtained rational function, it is possible to get the synthesis of an electric network which can be promptly included in the time-domain simulation. It is important to note that this electric circuit generates the same frequency response as the harmonic grounding impedance provided by HEM. Thus, it includes reactive and electromagnetic wave propagation effects.

5. Test cases

This section presents the test cases related to the comparison between two different grounding modeling, i.e., the low-frequency grounding resistance (R_{LF}) and the harmonic grounding impedance ($Z(\omega)$).

Let us consider a 1.2 km matched three-phase DL (Figure 1). The heights of the three-phase conductors are 10, 11 and 12 m respectively, while the shield wire is 14 m above the ground. The distance between each conductor and the shield wire is 2.4 m. The conductors' diameter is 1.83 cm, while the shield wire diameter is 0.72 cm.

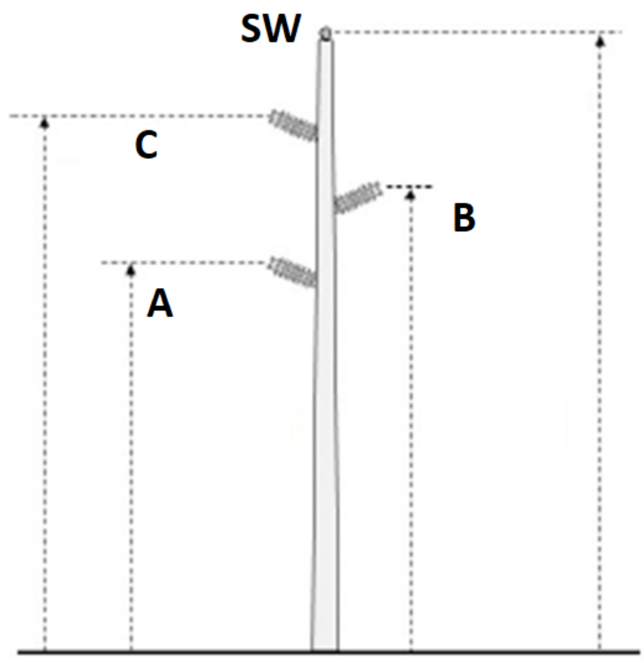

Figure 1. Line configuration

The span between each tower is 300 m, thus three towers placed at 300, 600 and 900 m from the beginning of the line are considered. Each tower is 14 m high and with a base diameter of 0.5 m. According to equation (3), a value of $Z_c = 244.17\ \Omega$ is considered. The propagation velocity along the tower is considered to be equal to the light speed.

Each tower is grounded with a grounding system as shown in Figure 2. This is a typical configuration for grounding distribution networks in the State of Minas Gerais, Brazil. It consists of three vertical rods 2.5 m long interconnected by a horizontal galvanized steel cable 6 m long. The vertical rods are copper-plated steel, with a diameter of 15 mm.

The equivalent circuit of the system composed of a three-phase distribution line, tower and grounding system is shown in figure 3.

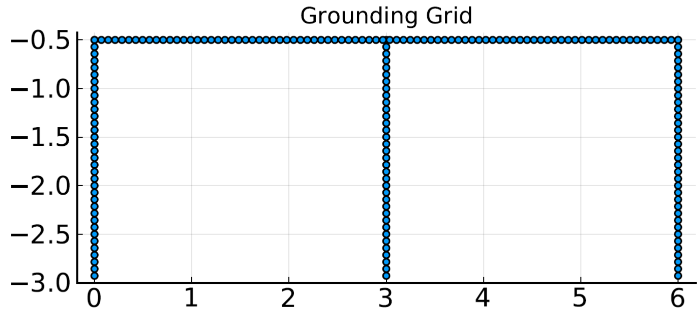

Figure 2. Grounding grid of the distribution tower

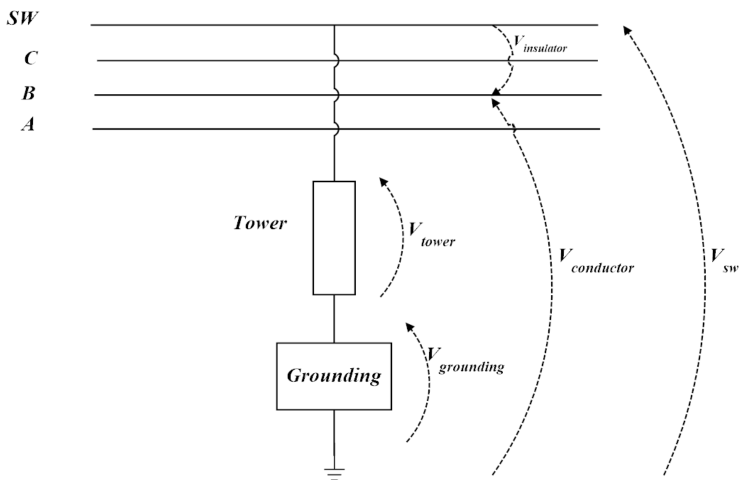

Figure 3. Equivalent circuit of the power system, tower and grouding

As will be discussed later, two different values of the soil conductivity will be considered (10 mS/m and 1 mS/m). This corresponds to two different grounding harmonic responses according to the grounding modeling proposed in Section 4. Figures 4-5 show $Z(\omega)$ and R_{LF} of the two considered cases. Based on the behaviors described in these figures, it is possible to verify that: i) grounding can only be represented by R_{LF} in the low-frequency range, where $Z(\omega)$ tends to R_{LF}; ii) the limit frequency of the low-frequency range increases with a reduction in conductivity; iii) in the intermediate-frequency range there is a predominance of capacitive behavior of the grounding, verified by the reduction of $Z(\omega)$ in relation to the R_{LF}; iv) the limit frequency of the intermediate-frequency range also increases with the decrease in conductivity and v) only in the high-frequency range there is a predominance of inductive effect, mainly for higher conductivity values. Thus, the response of the system under study (DL and grounding) will be a direct function of the frequency spectrum of the electromagnetic signal that requests it. As a consequence, it is expected that the overvoltages in the insulator string are sensitive to grounding modeling.

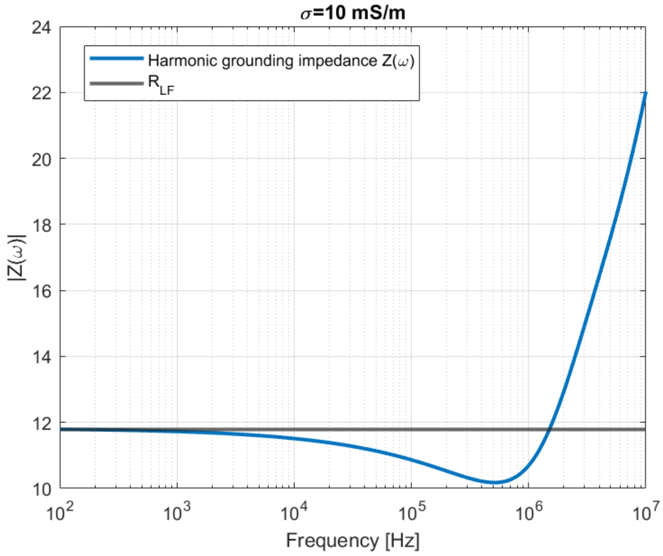

Figure 4. Grounding harmonic impedance $Z(\omega)$ with $\sigma = 10\ mS/m$

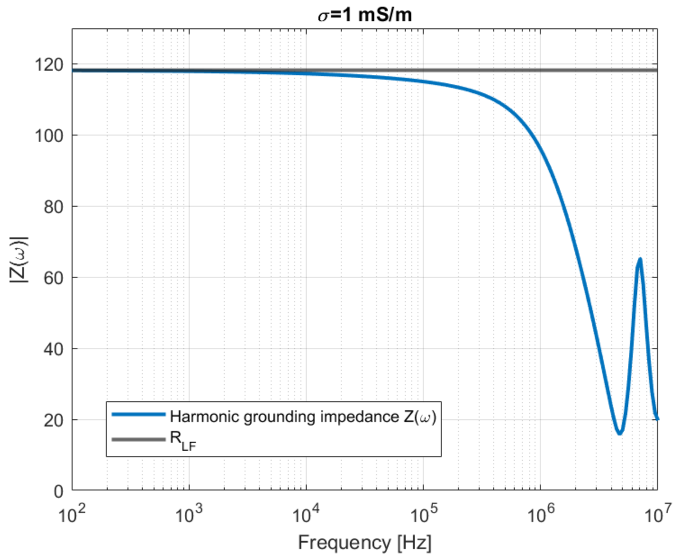

Figure 5. Grounding harmonic impedance $Z(\omega)$ with $\sigma = 1\ mS/m$

When we consider a grounding model described by R_{LF}, the implementation in the EMT-type software is trivial, while when we consider the harmonic grounding impedance, it is possible to obtain the synthesis of the electric circuit to be implemented in the EMT-type software thanks to the approach presented in Section 4.

The general layout of the circuit obtained from the Vector fitting approach is described in figure 6, while the values of the passive elements are proposed in Tables 1-2 for $\sigma = 10$ mS/m and $\sigma = 1$ mS/m, respectively. It is worth mentioning that this equivalent circuits are mathematical models that have a frequency response very close to $Z(\omega)$, but their electrical parameters do not have physical consistency. Hence the existence of negative values for resistance and inductance in Tables 1-2. The i-index appearing in Tables 1-2 refers to the electrical branch.

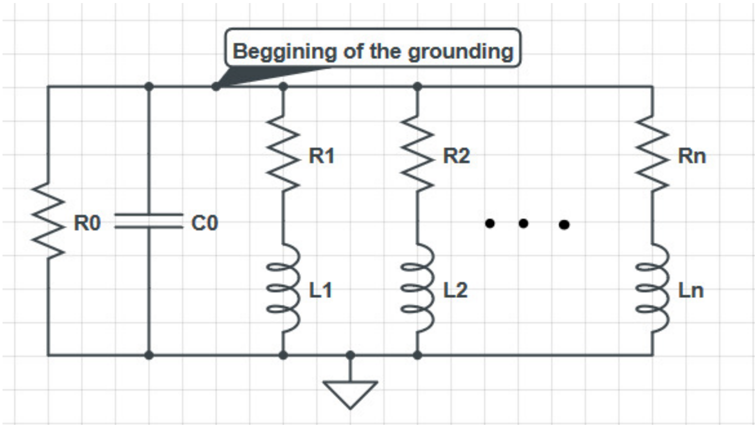

Figure 6. General layout of the grounding circuit for the harmonic grounding impedance

Table 1: Passive elements of the grounding circuit. $\sigma = 10$ mS/m

i	**Resistance** [Ω]	**Inductance** [mH]	**Capacitance** [μF]
0	3.33×10^{15}	-	3.00×10^{-10}
1	53.42	9.85×10^{-10}	-
2	5.24	7.20×10^{-4}	-
3	-6.97	-1.12×10^{-3}	-
4	-1.23×10^{2}	-7.69×10^{-2}	-
5	-2.66×10^{2}	-0.60	-
6	-5.14×10^{2}	-4.51	-
7	-9.98×10^{2}	-37.13	-
8	-1.99×10^{3}	-3.56×10^{2}	-
9	-3.83×10^{3}	-4.16×10^{3}	-
10	29.01	-4.07×10^{-5}	-

Table 2: Passive elements of the grounding circuit. $\sigma = 1$ mS/m

i	**Resistance** [Ω]	**Inductance** [mH]	**Capacitance** [μF]
0	3.33×10^{15}	-	3.00×10^{-10}
1	-2.06×10^{5}	$- 5.31 \times 10^{5}$	-
2	-1.55×10^{5}	-9.32×10^{4}	-
3	-9.54×10^{4}	-1.79×10^{4}	-
4	-5.80×10^{4}	-3.66×10^{3}	-
5	-3.58×10^{4}	-7.93×10^{2}	-
6	-2.26×10^{4}	-1.82×10^{2}	-
7	-1.46×10^{4}	-44.20	-
8	-9.89×10^{3}	-11.61	-
9	-7.53×10^{3}	-3.51	-
10	-8.34×10^{3}	-1.58	-
11	-5.69×10^{2}	-8.42×10^{-3}	-
12	-44.92	-9.42×10^{-5}	-

To compare the grounding modeling, 12 different tests have been implemented (Table 4), each one differing for the soil conductivity, stroke location and stroke type (first or subsequent). The stroke location is always placed in front of the middle of the line. The lightning return stroke channel is characterized by a height of 8 km and a speed equal to one-half the speed of light in vacuum. The channel-base current is modeled as a sum of two Heidler's functions as in equation 4, with parameters reported in Table 3.

$$I_0(t) = \frac{I_{01}}{\eta_1} \frac{\left(\frac{t}{\tau_{11}}\right)^{n_1}}{1 + \left(\frac{t}{\tau_{11}}\right)^{n_1}} e^{-\frac{t}{\tau_{12}}} + \frac{I_{02}}{\eta_2} \frac{\left(\frac{t}{\tau_{21}}\right)^{n_2}}{1 + \left(\frac{t}{\tau_{21}}\right)^{n_2}} e^{-\frac{t}{\tau_{22}}} \tag{4}$$

being

$$\eta_i = \exp\left(-\frac{\tau_{i1}}{\tau_{i2}}\left(n_i \frac{\tau_{i2}}{\tau_{i1}}\right)^{\frac{1}{n_i}}\right) \tag{5}$$

Table 3: Heidler's current parameters

Parameter	First	Subsequent
I_{01} [kA]	28.0	10.7
τ_{11} [μs]	1.8	0.22
τ_{12} [μs]	95.0	2.5
n_1	2	2
I_{02} [kA]	-	6.5
τ_{21} [μs]	-	2.1
τ_{22} [μs]	-	230.0
n_2	-	2

Table 4: Test details

Test	σ[S/m]	Stroke distance [m]	Stroke type
T1	0.01	60	First
T2	0.01	200	First
T3	0.01	2000	First
T4	0.001	60	First
T5	0.001	200	First
T6	0.001	2000	First
T7	0.01	60	Subsequent
T8	0.01	200	Subsequent
T9	0.01	2000	Subsequent
T10	0.001	60	Subsequent
T11	0.001	200	Subsequent
T12	0.001	2000	Subsequent

6. Results

In this section, the results for the test cases of Table 4 are presented showing the voltage across the phase B insulator string ($V_{insulator}$ in Figure 3) and the voltage difference occurring on the grounding system ($V_{grounding}$ in Figure 3).

Figures 7-12 show the results for tests T1-T6, corresponding to a typical first stroke. The main differences in terms of voltage across the insulator can be observed considering a low soil conductivity (figures 10-12) and for near stroke locations (60 m). This is extremely important because the closer the stroke location, the higher (and the more dangerous) the induced voltage. For example, let us consider Test T4 (figure 10). If we use the low-frequency grounding resistance (R_{LF}) as grounding model, the maximum induced voltage across the insulator string is 96.43 kV, while if we consider the harmonic grounding impedance ($Z(\omega)$), which represents in a better way the reality, the voltage is 121.70 kV. This clearly shows how the difference in the modeling could lead to either a fault or not across the insulator strings.

On the other side, when the harmonic grounding impedance model presents a voltage across the insulator higher with respect to the R_{LF} case, the voltage on the grounding system is lower. This can be explained as follows: let us consider Figure 3; the voltage difference occurring on the insulator string is

$$V_{insulator} = V_{conductor} - V_{sw} \tag{6}$$

It is reasonable to assume that the voltage on the conductor does not change in a meaningful way considering the two different grounding system modeling as the only difference is a different current flowing in the shield wire conductor, causing a different coupling with the phase conductor. Even if not negligible, the coupling between conductors does not represent the dominant aspect in the lightning-induced voltages (which is the electric field illuminating the conductor). Consequently, $V_{insulator} + V_{sw}$ is almost constant. The shield wire voltage is:

$$V_{sw} = V_{tower} + V_{grounding} \tag{7}$$

With the same current, V_{tower} is constant in the two cases but $V_{grounding}$ varies because the impedance varies according to Figures 4 and 5 for $\sigma = 10\ mS/m$ and $1\ mS/m$, respectively. Let us consider the most critical case, i.e., $\sigma = 1\ mS/m$: from Figure 5 it is clear that for each considered frequency $Z(\omega) < R_{LF}$, thus with the same current the voltage on the grounding system is lower if we consider the harmonic impedance $Z(\omega)$ and consequently also V_{sw} is lower. Since $V_{insulator} + V_{sw} = constant$, if V_{sw} decreases , $V_{insulator}$ increases. This aspect is confirmed in Tests T4-T5-T6, T10-T11-T12.

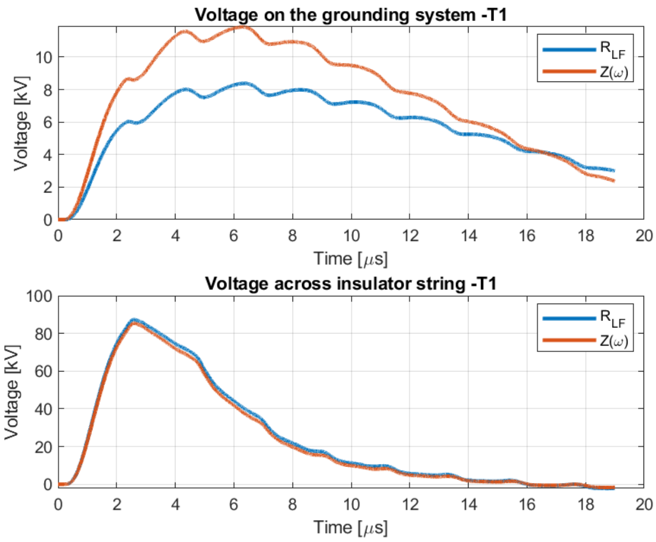

Figure 7. Test T1 - Voltage on the grounding system and on the insulator of phase B. Comparison between the two models

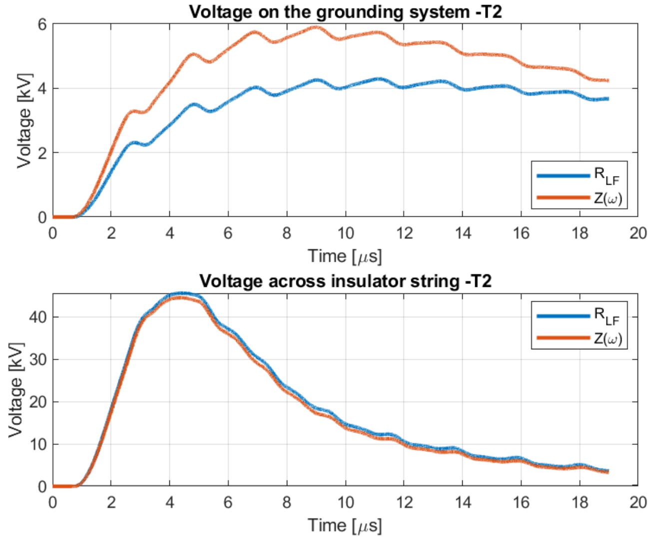

Figure 8. Test T2 - Voltage on the grounding system and on the insulator of phase B. Comparison between the two models

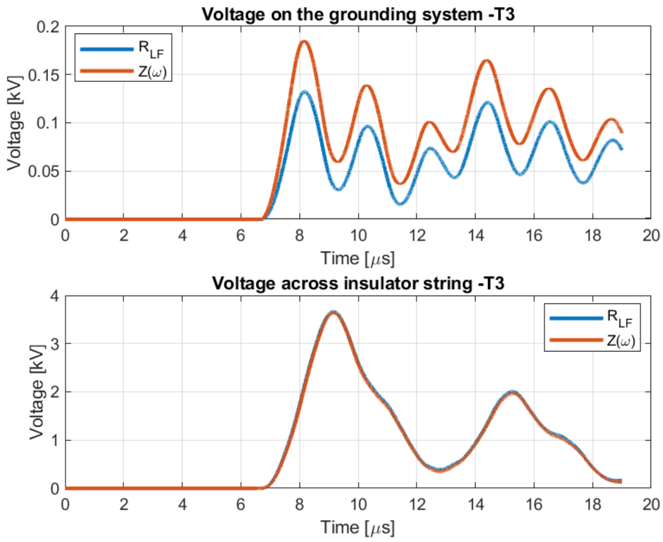

Figure 9. Test T3 - Voltage on the grounding system and on the insulator of phase B. Comparison between the two models

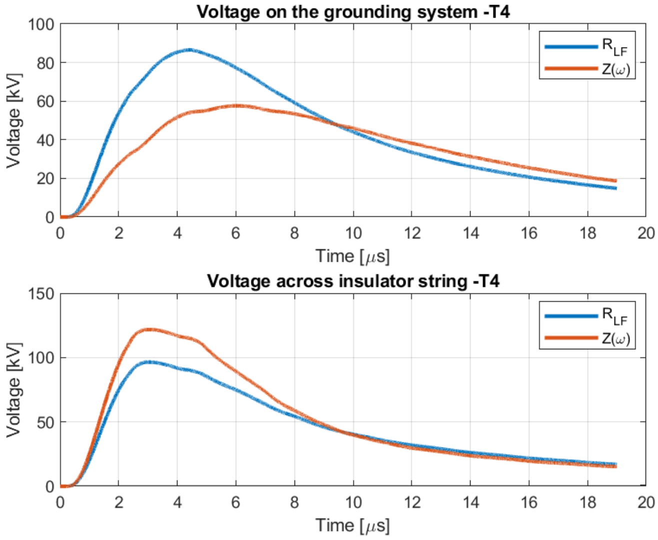

Figure 10. Test T4 - Voltage on the grounding system and on the insulator of phase B. Comparison between the two models

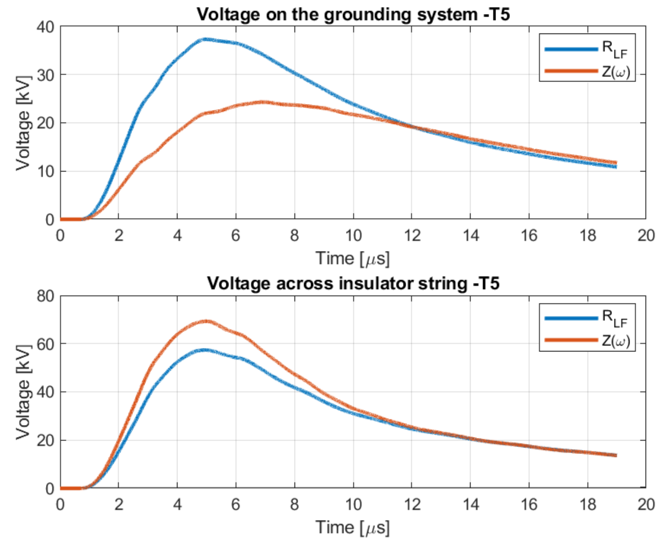

Figure 11. Test T5 - Voltage on the grounding system and on the insulator of phase B. Comparison between the two models

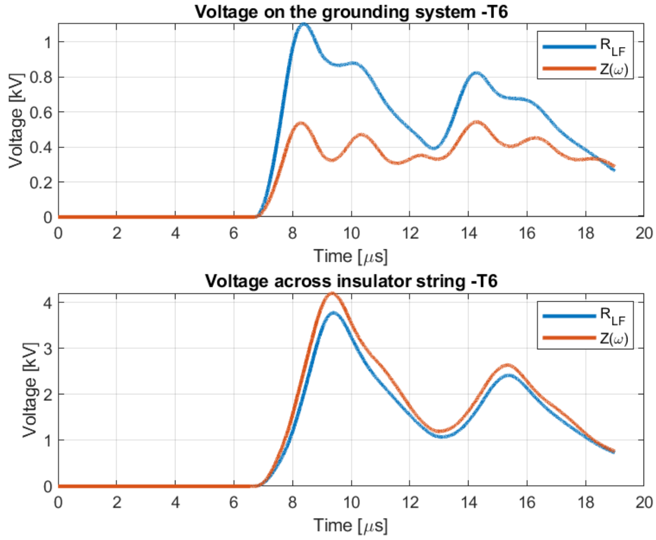

Figure 12. Test T6 - Voltage on the grounding system and on the insulator of phase B. Comparison between the two models

The results for subsequent strokes can be observed in Figures 13-18. The results are in agreement with the previous ones, confirming a significant increase of the maximum voltage if the equivalent circuit ($Z(\omega)$) is taken into account, especially if the soil conductivity is low.

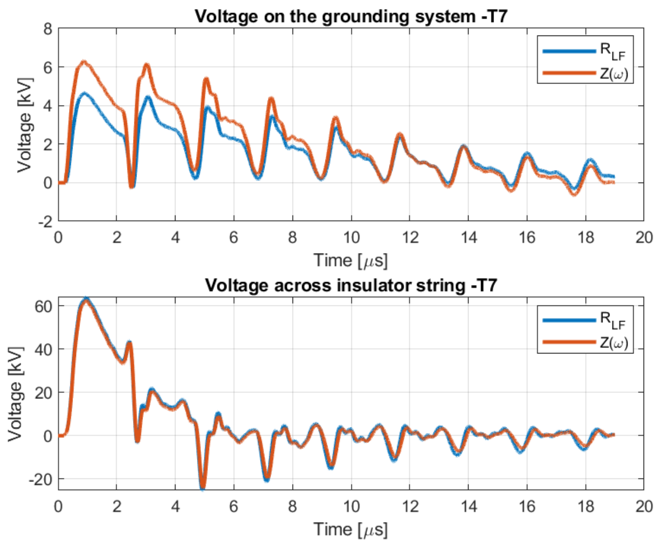

Figure 13. Test T7 - Voltage on the grounding system and on the insulator of phase B. Comparison between the two models

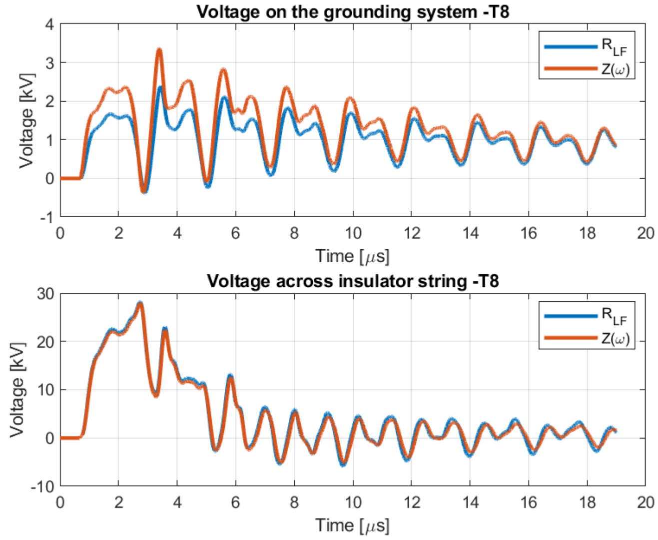

Figure 14. Test T8 - Voltage on the grounding system and on the insulator of phase B. Comparison between the two models

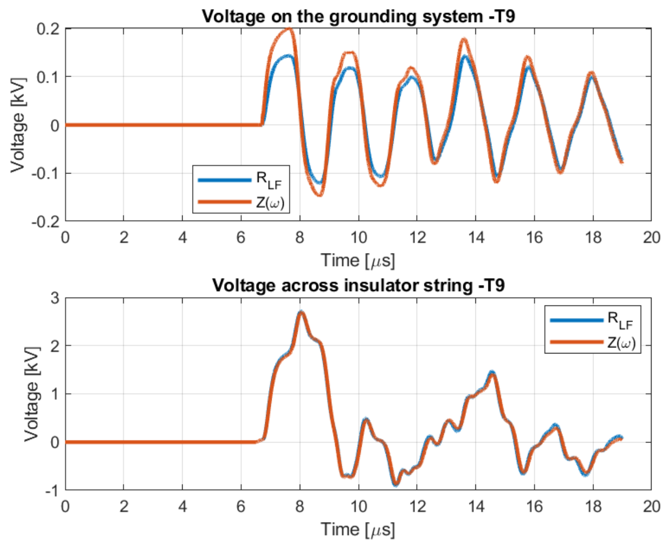

Figure 15. Test T9- Voltage on the grounding system and on the insulator of phase B. Comparison between the two models

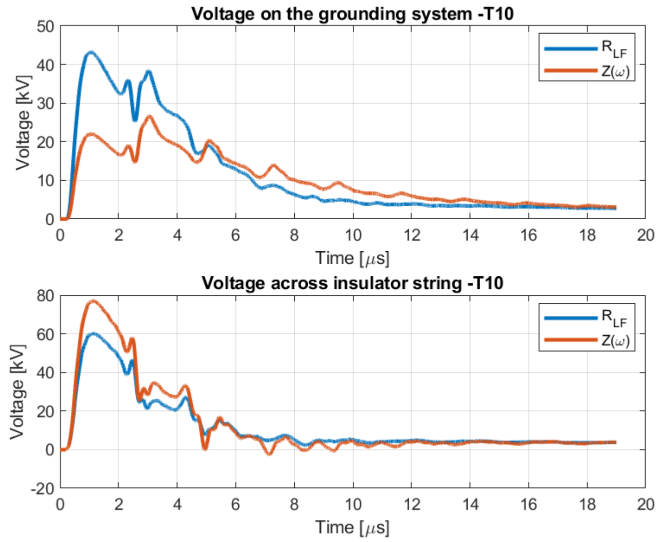

Figure 16. Test T10 - Voltage on the grounding system and on the insulator of phase B. Comparison between the two models

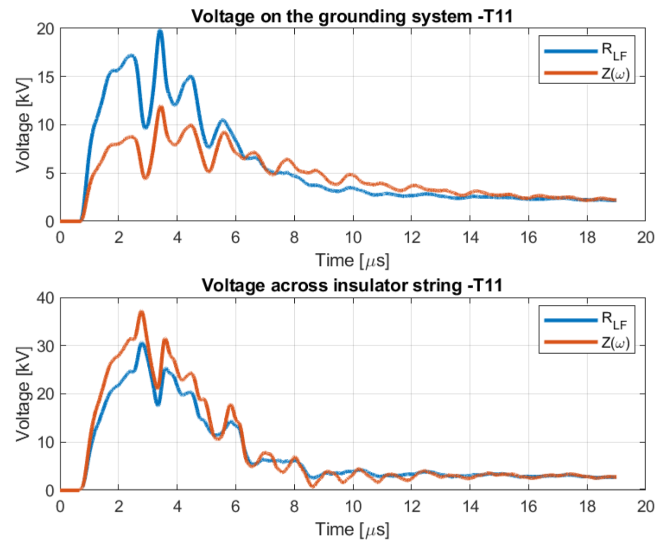

Figure 17. Test T11 - Voltage on the grounding system and on the insulator of phase B. Comparison between the two models

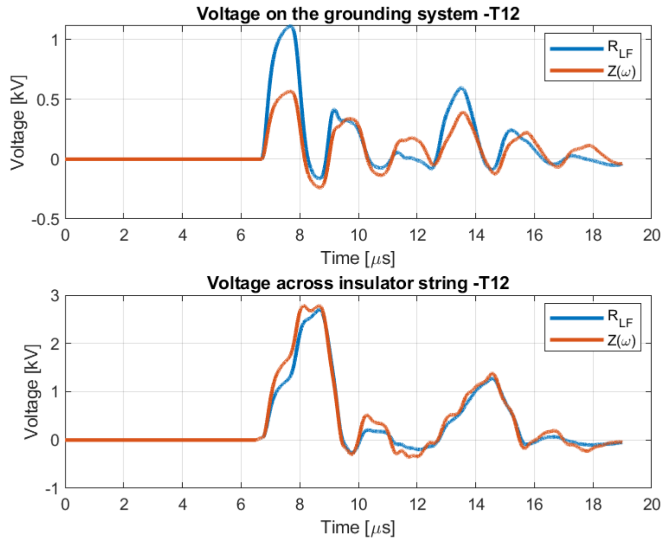

Figure 18. Test T12 - Voltage on the grounding system and on the insulator of phase B. Comparison between the two models

Finally, Table 5 shows the percentage increase in the maximum voltage across the phase B insulator considering the harmonic grounding impedance ($Z(\omega)$) with respect to the low-frequency grounding resistance (R_{LF}). According to the previous considerations, the differences are almost negligible if the soil conductivity is high (tests T1-T3 and T7-T9), but they become consistent when the soil conductivity decreases (tests T4-T6 and T10-T12). This behavior is more evident for close stroke location (test T4 and T10).

Table 5: Maximum voltage across the insulator. Percentage increase considering the harmonic grounding impedance ($Z(\omega)$) with respect to the low-frequency grounding resistance(R_{LF})

Test	**Voltage insulator increase [%]]**
T1	-2.57
T2	-2.81
T3	-0.62
T4	30.56
T5	22.72
T6	12.50
T7	-2.44
T8	-1.07
T9	-0.561
T10	33.61
T11	23.52
T12	3.17

7. Conclusions

Lightning induced-voltages are usually computed considering only the low-frequency grounding resistance when one considers the grounding system of the distribution tower. This work presented the impact of two different models for the grounding system of distribution line towers on the lightning-induced voltage on the phase insulators computation. The comparison between the low-frequency grounding resistance (R_{LF}) and the equivalent circuit corresponding to the wideband grounding frequency response ($Z(\omega)$) shows that considering only R_{LF} may lead to not-negligible underestimation of the maximum induced voltage. This aspect is more evident for both first and subsequent strokes in the case of close stroke locations and low soil conductivities, which represents, by the way, one of the configurations when the lightning-induced voltages on a distribution line are high and potentially dangerous. On the other hand, for high soil conductivity the differences between the two models are negligible. Future work will extend this analysis to the evaluation of a distribution line lightning performance to check whether this trend is also confirmed when dealing with statistical calculations.

Author Contributions: Conceptualization, Daniele Mestriner and Rodolfo Moura; methodology, Daniele Mestriner; software, Renato Procopio and Rodolfo Moura; validation, Daniele Mestriner and Marco Schroeder; formal analysis, Daniele Mestriner and Marco Schroeder; writing—original draft preparation, Daniele Mestiner and Rodolfo Moura; writing—review and editing, Renato Procopio and Marco Schroeder; All authors have read and agreed to the published version of the manuscript.

Funding: This research received no external funding

Institutional Review Board Statement: Not applicable

Informed Consent Statement: Not applicable

Conflicts of Interest: The authors declare no conflict of interest

References

1. Cooray, V.; Scuka, V. Lightning-induced overvoltages in power lines: validity of various approximations made in overvoltage calculations. *IEEE Transactions on Electromagnetic Compatibility* **1998**, *40*, 355–363. doi:10.1109/15.736222.
2. Borghetti, A.; Nucci, C.A.; Paolone, M. An Improved Procedure for the Assessment of Overhead Line Indirect Lightning Performance and Its Comparison with the IEEE Std. 1410 Method. *IEEE Transactions on Power Delivery* **2007**, *22*, 684–692. doi:10.1109/TPWRD.2006.881463.
3. Ren, H.; Zhou, B.; Rakov, V.A.; Shi, L.; Gao, C.; Yang, J. Analysis of Lightning-Induced Voltages on Overhead Lines Using a 2-D FDTD Method and Agrawal Coupling Model. *IEEE Transactions on Electromagnetic Compatibility* **2008**, *50*, 651–659. doi:10.1109/TEMC.2008.926910.
4. Paulino, J.O.S.; Barbosa, C.F.; Lopes, I.J.S.; d. C. Boaventura, W. An Approximate Formula for the Peak Value of Lightning-Induced Voltages in Overhead Lines. *IEEE Transactions on Power Delivery* **2010**, *25*, 843–851. doi:10.1109/TPWRD.2009.2035319.
5. IEEE Guide for Improving the Lightning Performance of Electric Power Overhead Distribution Lines. *IEEE Std 1410-2010 (Revision of IEEE Std 1410-2004)* **2011**, pp. 1–73. doi:10.1109/IEEESTD.2011.5706451.
6. Silveira, F.H.; De Conti, A.; Visacro, S. Voltages Induced in Single-Phase Overhead Lines by First and Subsequent Negative Lightning Strokes: Influence of the Periodically Grounded Neutral Conductor and the Ground Resistivity. *IEEE Transactions on Electromagnetic Compatibility* **2011**, *53*, 414–420. doi:10.1109/TEMC.2011.2106134.
7. Paulino, J.O.S.; Barbosa, C.F.; Lopes, I.J.S.; d. C. Boaventura, W. The Peak Value of Lightning-Induced Voltages in Overhead Lines Considering the Ground Resistivity and Typical Return Stroke Parameters. *IEEE Transactions on Power Delivery* **2011**, *26*, 920–927. doi:10.1109/TPWRD.2010.2095887.
8. Andreotti, A.; Pierno, A.; Rakov, V.A. An Analytical Approach to Calculation of Lightning Induced Voltages on Overhead Lines in Case of Lossy Ground—Part II: Comparison With Other Models. *IEEE Transactions on Power Delivery* **2013**, *28*, 1224–1230. doi:10.1109/TPWRD.2013.2241085.
9. Paulino, J.; Barbosa, C.; Lopes, I.; Boaventura, W. Assessment and analysis of indirect lightning performance of overhead lines. *Electric Power Systems Research* **2015**, *118*, 55 – 61. The Lightning Flash and Lightning Protection (SIPDA 2013), doi:https://doi.org/10.1016/j.epsr.2014.07.016.
10. Borghetti, A.; Napolitano, F.; Nucci, C.A.; Tossani, F. Influence of the return stroke current waveform on the lightning performance of distribution lines. 2017 IEEE Power Energy Society General Meeting, 2017, pp. 1–1. doi:10.1109/PESGM.2017.8274003.
11. Piantini, A. Extension of the Rusck Model for Calculating Lightning-Induced Voltages on Overhead Lines Considering the Soil Electrical Parameters. *IEEE Transactions on Electromagnetic Compatibility* **2017**, *59*, 154–162. doi:10.1109/TEMC.2016.2601011.
12. Piantini, A. Analysis of the effectiveness of shield wires in mitigating lightning-induced voltages on power distribution lines. *Electric Power Systems Research* **2018**, *159*, 9 – 16. Recent Developments on Lightning Research and Protection Technologies, doi:https://doi.org/10.1016/j.epsr.2017.08.022.
13. Paulino, J.O.S.; Barbosa, C.F. Effect of high-resistivity ground on the lightning performance of overhead lines. *Electric Power Systems Research* **2019**, *172*, 253 – 259. doi:https://doi.org/10.1016/j.epsr.2019.03.026.
14. Paulino, J.O.S.; Barbosa, C.F. On Lightning-Induced Voltages in Overhead Lines Over High-Resistivity Ground. *IEEE Transactions on Electromagnetic Compatibility* **2019**, *61*, 1499–1506. doi:10.1109/TEMC.2018.2856751.
15. Andreotti, A.; Araneo, R.; Mahmood, F.; Piantini, A.; Rubinstein, M. An Analytical Approach to Assess the Influence of Shield Wires in Improving the Lightning Performance due to Indirect Strokes. *IEEE Transactions on Power Delivery* **2020**, pp. 1–1. doi:10.1109/TPWRD.2020.3009886.
16. Brignone, M.; Mestriner, D.; Procopio, R.; Piantini, A.; Rachidi, F. Evaluation of the Mitigation Effect of the Shield Wires on Lightning Induced Overvoltages in MV Distribution Systems Using Statistical Analysis. *IEEE Transactions on Electromagnetic Compatibility* **2018**, *60*, 1400–1408. doi:10.1109/TEMC.2017.2779184.

17. Schroeder, M.A.O.; de Barros, M.T.C.; Lima, A.C.; Afonso, M.M.; Moura, R.A. Evaluation of the impact of different frequency dependent soil models on lightning overvoltages. *Electric Power Systems Research* **2018**, *159*, 40 – 49. Recent Developments on Lightning Research and Protection Technologies, doi:https://doi.org/10.1016/j.epsr.2017.09.020.
18. Visacro, S.; Soares, A.; Schroeder, M. An interactive computational code for simulation of transient behavior of electric system components for lightning currents. Proc. 26th Int. Conf. Lightning Protection, 2002, pp. 732–737.
19. Visacro, S.; Soares, A. HEM: a model for simulation of lightning-related engineering problems. *IEEE Transactions on Power Delivery* **2005**, *20*, 1206–1208. doi:10.1109/TPWRD.2004.839743.
20. Gustavsen, B.; Semlyen, A. Rational approximation of frequency domain responses by vector fitting. *IEEE Transactions on Power Delivery* **1999**, *14*, 1052–1061. doi:10.1109/61.772353.
21. Gustavsen, B. Fast Passivity Enforcement for Pole-Residue Models by Perturbation of Residue Matrix Eigenvalues. *IEEE Transactions on Power Delivery* **2008**, *23*, 2278–2285. doi:10.1109/TPWRD.2008.919027.
22. Brignone, M.; Delfino, F.; Procopio, R.; Rossi, M.; Rachidi, F. Evaluation of Power System Lightning Performance, Part I: Model and Numerical Solution Using the PSCAD-EMTDC Platform. *IEEE Transactions on Electromagnetic Compatibility* **2017**, *59*, 137–145. doi:10.1109/TEMC.2016.2601640.
23. Farina, L.; Mestriner, D.; Procopio, R.; Brignone, M.; Delfino, F. The Lightning Power Electromagnetic simulator for Transient Overvoltages (LIGHT-PESTO) code: an user-friendly interface with the Matlab-Simulink environment. *IEEE Letters on Electromagnetic Compatibility Practice and Applications* **2020**, pp. 1–1. doi:10.1109/LEMCPA.2020.3032180.
24. Brignone, M.; Procopio, R.; Mestriner, D.; Rossi, M.; Delfino, F.; Rachidi, F.; Rubinstein, M. Analytical Expressions for Lightning Electromagnetic Fields With Arbitrary Channel-Base Current—Part I: Theory. *IEEE Transactions on Electromagnetic Compatibility* **2020**, pp. 1–9. doi:10.1109/TEMC.2020.3018199.
25. Mestriner, D.; Brignone, M.; Procopio, R.; Rossi, M.; Delfino, F.; Rachidi, F.; Rubinstein, M. Analytical Expressions for Lightning Electromagnetic Fields With Arbitrary Channel-Base Current. Part II: Validation and Computational Performance. *IEEE Transactions on Electromagnetic Compatibility* **2020**, pp. 1–8. doi:10.1109/TEMC.2020.3018108.
26. Agrawal, A.K.; Price, H.J.; Gurbaxani, S.H. Transient response of multiconductor transmission lines excited by a nonuniform electromagnetic field. *IEEE Transactions on electromagnetic compatibility* **1980**, pp. 119–129.
27. Rachidi, F.; Loyka, S.; Nucci, C.; Ianoz, M. A new expression for the ground transient resistance matrix elements of multiconductor overhead transmission lines. *Electric Power Systems Research* **2003**, *65*, 41–46.
28. Sargent, M.A.; Darveniza, M. Tower Surge Impedance. *IEEE Transactions on Power Apparatus and Systems* **1969**, *PAS-88*, 680–687. doi:10.1109/TPAS.1969.292357.
29. Martinez-Velasco, J.A. *Power System Transients: Parameter Determination*, first ed.; CRC Press, 2010.
30. Electromagnetic computation methods for lightning surge studies with emphasis on the FDTD method. *Cigré, Technical Brochures 785* **2019**, *WG C4.37*, 1–192.
31. Alipio, R.; Visacro, S. Modeling the Frequency Dependence of Electrical Parameters of Soil. *IEEE Transactions on Electromagnetic Compatibility* **2014**, *56*, 1163–1171. doi:10.1109/TEMC.2014.2313977.
32. Alipio, R.; Visacro, S. Impulse Efficiency of Grounding Electrodes: Effect of Frequency-Dependent Soil Parameters. *IEEE Transactions on Power Delivery* **2014**, *29*, 716–723. doi:10.1109/TPWRD.2013.2278817.
33. Visacro, S.; Alipio, R.; Pereira, C.; Guimarães, M.; Schroeder, M.A.O. Lightning Response of Grounding Grids: Simulated and Experimental Results. *IEEE Transactions on Electromagnetic Compatibility* **2015**, *57*, 121–127. doi:10.1109/TEMC.2014.2362091.
34. Kuhar, A.; Arnautovski-Toševa, V.; Grčev, L. HIGH FREQUENCY ENHANCEMENT OF THE HYBRID ELECTROMAGNETIC MODEL BY IMPLEMENTING COMPLEX IMAGES. *Journal of Electrical Engineering and Information Technologies* **2017**, *2*, 79–87.
35. Kuhar, A.; Arnautovski-Toševa, V.; Ololoska-Gagoska, L.; Grčev, L.; Markovski, B. INFLUENCE OF SEGMENTATION ON THE PRECISION OF CIRCUIT BASED METHODS. *Journal of Electrical Engineering and Information Technologies* **2018**, *3*, 148.
36. de Oliveira Schroeder, M.A.; de Moura, R.A.R.; Machado, V.M. A Discussion on Practical Limits for Segmentation Procedures of Tower-Footing Grounding Modeling for Lightning Responses. *IEEE Transactions on Electromagnetic Compatibility* **2020**, *62*, 2520–2527. doi:10.1109/TEMC.2020.2982358.
37. Harrington, R.F. *Field Computation by Moment Methods*; Wiley-IEEE Press, 1993.
38. Grcev, L.; Grceva, S. On HF circuit models of horizontal grounding electrodes. *IEEE Transactions on Electromagnetic Compatibility* **2009**, *51*, 873–875.
39. Arnautovski-Toseva, V.; Grcev, L. On the Image Model of a Buried Horizontal Wire. *IEEE Transactions on Electromagnetic Compatibility* **2016**, *58*, 278–286.